Nuclear Inst. and Methods in Physics Research, A 961 (2020) 163601

Contents lists available at ScienceDirect

Nuclear Inst. and Methods in Physics Research, A

journal homepage: www.elsevier.com/locate/nima

Performance of 5-μm PIN diamond diodes as thermal neutron detectors

Jason Holmes [a], Jesse Brown [a], Franz A. Koeck [a], Holly Johnson [a], Manpuneet K. Benipal [b], Praneeth Kandlakunta [c], Anna Zaniewski [a], Ricardo Alarcon [a,*], Raymond Cao [c], Stephen M. Goodnick [d], Robert J. Nemanich [a]

[a] Department of Physics, Arizona State University, Tempe, AZ 85287-1504, United States of America
[b] ADVENT Diamond Inc., Phoenix, Arizona, United States of America
[c] Nuclear Engineering Program, Department of Mechanical and Aerospace Engineering, The Ohio State University, Columbus, OH 43221, United States of America
[d] School of Electrical, Computer and Energy Engineering, Arizona State University, Tempe, AZ 85287-9309, United States of America

ARTICLE INFO

Keywords:
Neutron detection
Diamond detector
PIN diode
Boron nitride
Radiation hardness

ABSTRACT

Diamond PIN diodes with an approximately 5-μm thick i-layer and coated with a thin boron nitride (BN) layer have been tested with a thermal neutron beam. For a flux of 4.4×10^6 n/s/cm^2, count rates were on the order of 30–100 counts per second depending on the thickness of the BN neutron converter layer. Pulse height spectra showed features associated with α and ^{7}Li fission products consistent with the thickness of the BN layer. An irradiation test with a 1 MeV neutron equivalent fluence of 10^{15} n/cm^2 showed no significant alteration in the count rate of the tested detector.

1. Introduction

Thin-film coated semiconductor thermal neutron detectors offer a compact technology for high flux applications [1,2]. The neutron detection efficiency is limited due to self-absorption effects in the conversion layer and several methods can be employed to attain higher efficiencies [3,4]. For monitoring fluxes at nuclear reactors or at intense neutron beams, low neutron detector efficiency (<1%) is more desirable as it allows for linear pulse counting capabilities. However, radiation damage to the semiconductor could limit the detector optimum operation [5].

Diamond has very promising properties for a radiation detector and diamond detectors under α-particle irradiation have shown 100% charge collection efficiency with an energy resolution <1% [6]. The properties of diamond that contribute to its value in radiation detection include wide bandgap (5.5 eV), high electron and hole mobilities, high breakdown field, and high displacement damage threshold. These properties combine to enable radiation hard, low background, relatively efficient particle detectors. We have developed and demonstrated diamond p-i-n (PIN) diode particle detectors based on epitaxial growth of n-type, phosphorus doped diamond, high purity undoped (intrinsic) diamond, and p-type, boron doped diamond [7]. The detector i-layer thickness has been adjusted to match the penetration depth of designated α-particles, which minimizes background due to gamma radiation and high energy particles. Moreover, the detectors can be operated in pulse mode with a bias of only a few volts. The unique properties of the p-i-n diode led to the development of a new method to mitigate the polarization effect [8].

The conversion of thermal neutrons into directly detectable particles is best accomplished with the ^{10}B(n, α) reaction which can be written as [9]

$$ {}^{10}_{5}B + {}^{1}_{0}n \rightarrow \begin{cases} {}^{7}_{3}Li + {}^{4}_{2}\alpha & (ground\ state) \\ {}^{7}_{3}Li^{\cdot} + {}^{4}_{2}\alpha & (excited\ state) \end{cases} $$

The branching Q-values are 2.792 MeV and 2.310 MeV, respectively. With thermal neutrons about 94% of all reactions lead to the excited state and only 6% directly to the ground state. The reaction products are emitted in exactly opposite directions sharing the energy always in the same manner such that for the 94% branching ratio $E_{Li} = 0.84$ MeV and $E_{\alpha} = 1.47$ MeV.

Building on the results previously obtained with a p-i-n diamond detector [7], where α-detection was accomplished with no significant background and with negligible sensitivity to gamma radiation, this paper presents results obtained from tests of thermal neutron detectors developed through the integration of a boron nitride (BN) neutron absorption layer and an optimized diamond p-i-n detector. Like diamond, boron nitride is a hard, high temperature material that is expected to survive in extreme environments. A number of BN/diamond PIN neutron detectors have been fabricated at Arizona State University and tested with consistent results at The Ohio State University Nuclear

* Corresponding author.
E-mail address: ricardo.alarcon@asu.edu (R. Alarcon).

https://doi.org/10.1016/j.nima.2020.163601
Received 17 December 2019; Received in revised form 3 February 2020; Accepted 4 February 2020
Available online 7 February 2020

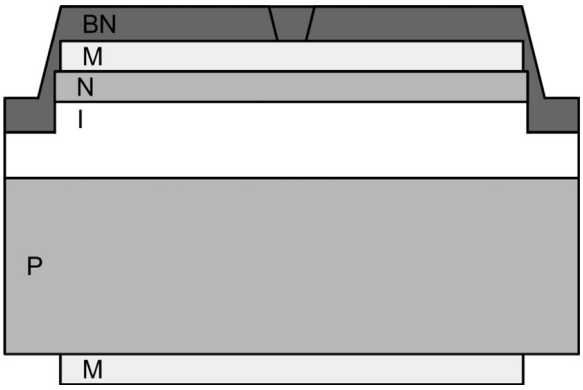

Fig. 1. Detector schematic. A cross-sectional view of the detector (not at scale) showing the layers labeled *BN*: boron nitride layer, *M*: Ti/Pt/Au contacts, *N*: n-type (P) diamond, I; intrinsic diamond, and *P*: p-type (B) diamond.

Reactor Laboratory (OSU-NRL). The tests include pulse counting measurements at a thermal neutron beamline with a flux of 4.4 × 10^6 n/cm^2/s, and irradiation of the detectors in the reactor core to a 1-MeV neutron equivalent fluence of 10^{15} n/cm^2.

2. Detector fabrication

2.1. The PIN diodes

A schematic of the complete detector is shown in Fig. 1. The PIN detector diodes were prepared using 3 mm × 3 mm × 0.3 mm high-pressure, high-temperature (HPHT), boron doped substrates with a boron concentration of ~1.2 × 10^{20} cm^{-3}. With a crystallographic (111) orientation and minimum miscut angle of ±1.5 deg, the surface was polished to an RMS roughness of ~40 nm. The growth of the diamond PIN substrate has been described in a previous paper [7].

Following the growth of the PIN wafer, electrical contacts were deposited with the following steps. First, the sample was cleaned via a 20 min hot acid etch in H_2SO_4/HNO_3 4:1 followed by 20 min off heat (in acid bath) and 5 min of running deionized (DI) water. Subsequently, a photoresist mask was patterned on the n-layer side (LOR3A, 12,000RPM spin coat). A surface descum process employed an oxygen-based plasma prior to deposition of a 500 nm aluminum (Al) film (Lesker PVD75 e-beam). The lift-off process was used to create a hard mask for a subsequent etching step. The remaining photoresist areas were lifted off and the sample was etched 1 μm into the intrinsic layer using an oxygen plasma. The Al mask was then removed (AZ400T/water bath). The cleaning and photoresist steps were repeated prior to the lift-off process that defined the final contacts (Ti/Pt/Au: 50 nm/50 nm/150 nm).

2.2. The BN neutron conversion layers

The BN layer was deposited on top of the electrical contacts using an electron cyclotron resonance (ECR) microwave plasma chemical vapor deposition (ECR MP CVD). The deposition chamber maintains a base pressure of ~3 × 10^{-9} Torr, monitored by a cold cathode gauge. An ASTeX 1500i microwave generator operated at 1.4 kW with a frequency of 2.45 GHz, coupled with a magnetic field of ~875 G applied by two ASTeX ECR magnets were used to ignite a plasma from the precursor gas. A gas mixture of He/Ar / N_2 / H_2 / BF_3 was introduced below the ECR Magnets. A toroidal tungsten coil beneath the substrate radiatively heated the sample to 505 ± 5 °C, monitored with a Mikron M90Q optical pyrometer. During deposition a negative bias $V_{applied}$ = −30 V was applied to the sample holder and substrate, relative to the chamber walls. The ion impact with the substrate was measured during deposition by monitoring the current through the substrate.

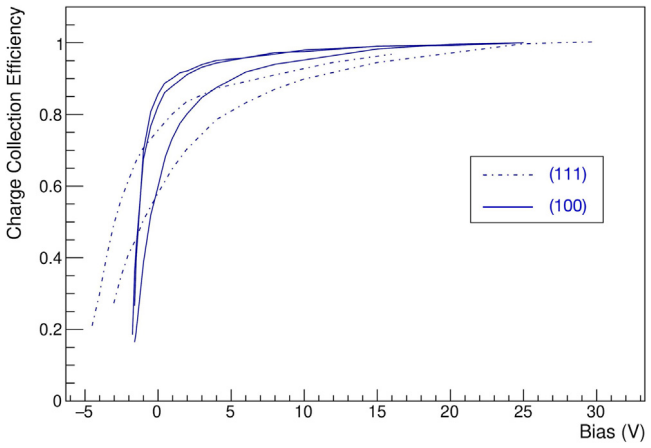

Fig. 2. Charge collection. The charge collection efficiencies shown for the constructed detectors as a function of the applied voltage. The solid lines correspond to detectors with a ⟨100⟩ crystal orientation and the dashed to detectors with a ⟨111⟩ crystal orientation.

The thickness of the BN conversion layer is limited by the range of the 1.47 MeV α-particle (4.25 μm) and the growth rates for BN by standard methods such as sputtering were too slow for practical device fabrication. The growth mechanism proposed in prior studies [10–12] suggested the active growth species of BN is BF_x and NH_x. We found that increasing the flow of BF_3 and H_2 the reaction will shift toward the products and increase the growth rate. To determine the growth rate, we used p-type silicon wafers with the same titanium, platinum, gold structure on the surface to mimic the contact pad of the detectors. Both *in-situ* X-ray photoelectron spectroscopy and *ex-situ* ellipsometry were used to measure a growth rate of 3.7 ± 0.7 nm/min [13].

Using the parameters in Table 1, a BN layer of 445 ± 89 nm was deposited on the sample that underwent thermal neutron beam and irradiation tests (Sections 3 and 4). After BN deposition, silver epoxy was used to make electrical contact and adhere the back side of the detector to a printed circuit board. A nano-milling process using an AFM with a single crystal diamond tip, was used to remove a 90 × 180 μm^2 area of BN and expose the gold contact below. Finally, gold wires were used to wire bond from this exposed contact pad to the printed circuit board.

2.3. Detector characterization with an α-source

The charge collection efficiency for each diamond detector was measured with a ^{210}Po α-source before the BN layer was added. Two diamonds were of ⟨111⟩ orientation and three were of ⟨100⟩ orientation. The growth process and testing apparatus has been previously described [6] and the charge collection efficiency results are shown in Fig. 2. The ⟨100⟩ diamonds (blue) are seen to be consistent in their response and very quickly saturating. The ⟨111⟩ diamonds are slower to saturate. In addition, although the quantities are small, the ⟨111⟩ diamonds were more prone to inoperability as a detector after being instrumented. It is unknown whether the growth process or something intrinsic to the diamond orientation causes these differences. Due to the good performance and reproducibility of the ⟨100⟩ diamonds, the neutron testing described next was focused on the best performing ⟨100⟩ diamond detector.

3. Thermal neutron beam measurements

Described here are measurements using a thermal neutron beamline at the 500 kWth research reactor facility at OSU-NRL. The beamline delivers a thermal equivalent neutron flux of 4.4 ×10^6 n/s/cm^2, with a circular beam size of 3-cm diameter, when reactor is operated at

Table 1
Processing parameters used to prepare the sample that is presented in Section 3.

	Temp °C	Pressure (Torr)	Power (W)	Bias (V)	Time (h)	He (sccm)	Ar (sccm)	N_2 (sccm)	H_2 (sccm)	BF_3 (sccm)
Cleaning	300	6×10^{-5}	300	–	0.5	–	2.5	–	20	–
Deposition	500	4×10^{-5}	1400	−30	2	35	2.5	12.5	20	4

Fig. 3. Detector mount. The detector frames made out of printed circuit boards with the detector centered at the tip of the frame.

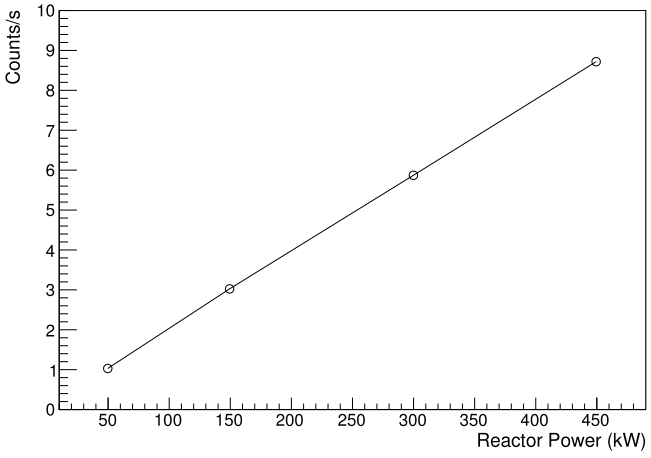

Fig. 5. Linear count rate. The count rates in counts/s for a detector versus the reactor power.

450 kWth. Fig. 3 shows the array of detectors including spares that were prepared for the tests. Some of these were tested sequentially with the neutron beam. Each detector frame was mounted about 10 cm from the port on a motor-controlled two-dimensional arm with mm-precision scanning capabilities. The detector frames are made out of printed circuit boards with the detector centered at the tip of the frame. The wider part of the frame handles mounting and signal transport. The detectors were read out using an ORTEC-based pulse counting electronics system. The signal connection was fed into an ORTEC 142A preamplifier and the output connected to an ORTEC 672 spectroscopy amplifier. The n-side of the diamond diode was biased between −3 V and 45 V relative to the p-side (reverse bias is positive) using the ORTEC 428 detector bias supply. The p-side was biased to ground and the response to the neutron induced reaction products from the BN layer was measured from the n-side.

Measurement of the neutron beam profile was performed by scanning a detector using 5 mm motor steps in the horizontal and vertical directions. The results are shown in Fig. 4 and agree well with the profiles obtained with a neutron imaging apparatus used by the facility [14]. Fig. 5 shows the linear behavior of the count rate versus the reactor power for one of the detectors.

Fig. 6 shows the pulse height distribution obtained with a ⟨100⟩ diamond diode that was coated with a BN layer approximately 0.5 μm thick. This relatively thin thickness offers the diamond detectors opportunities to distinguish energy peaks formed by individual reaction products from boron neutron capture. The pulse counting rate above threshold was around 40 counts/s. The maximum conversion efficiency (signal/neutron) for a single ^{10}B layer can be calculated from the known absorption cross section and the geometry of the arrangement and it is about 6% when the thickness of the conversion layer is close to the range in ^{10}B of the 1.47 MeV alpha particle, approximately 3.9 μm [15]. This range in turn is about eight times larger than the 0.5 μm thickness of the BN layer. Thus, the estimated theoretical efficiency of the detector in Fig. 6 is about 0.1% after correcting for

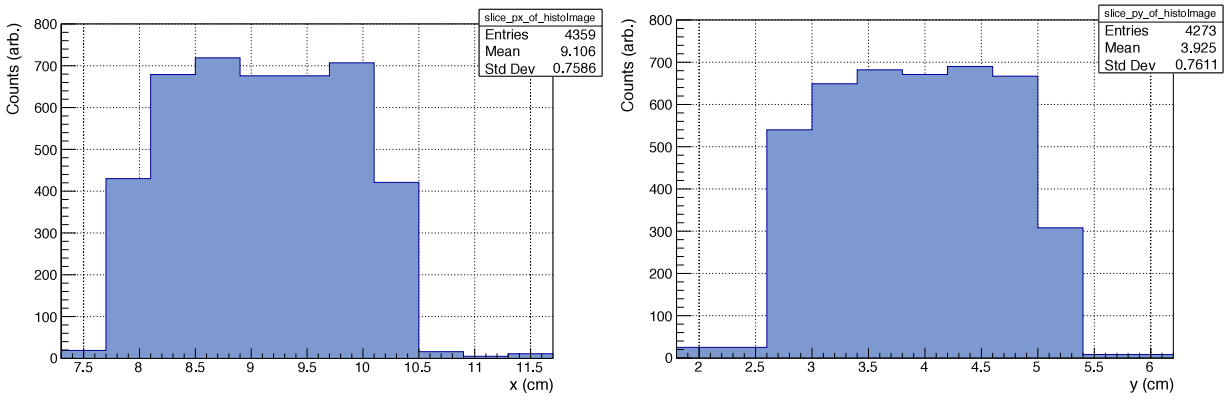

Fig. 4. Beam profile. The beam profile measured by horizontal and vertical scans of the thermal neutron beam in 5 mm steps.

the layer thickness and the chemical composition of the BN layer. The estimated experimental efficiency of the detector in Fig. 6 was about 0.03% in agreement with other reported experimental efficiencies being smaller than the calculated ones [15].

In Fig. 6, two most prominent peaks (around channels 35 and 85 respectively) correspond to the 94% branching ratio of the ^{10}B(n, α)^{7}Li capture reaction by which a ^{7}Li nuclei with 0.84 MeV kinetic energy is released in coincidence with a 1.47 MeV α-particle. The peak around channel 105 corresponds to the 1.78 MeV α-particle from the 6% branching ratio with the accompanying ^{7}Li nuclei of 1.01 MeV kinetic energy being part of the background curve centered around channel 50. In the low channel region 584 keV protons from the ^{14}N(n,p)^{14}C contribute insignificantly to the signal, because of self-absorption and the low ^{14}N neutron capture cross-section (1.83 barn for thermal neutrons) compared to ^{10}B neutron capture (3842 barn for thermal neutrons). The use of thicker BN layers produces similar curves to that of Fig. 6 but with less pronounced characteristics as the main ^{7}Li peak is very close to the electronics threshold.

The decay products of the ^{10}B(n,α)^{7}Li reaction lose a fraction of their kinetic energy when they travel through part of the 0.5 μm BN layer. After correcting for this energy loss, the identifiable peaks of Fig. 6 have a linear relation with a slope of $15.0^{+2.5}_{-1.6}$ keV/channel (95% confidence interval).

4. Irradiation results

For fluences of 1-MeV neutron equivalent of about 10^{15} n/cm^2 diamond-based detectors have been reported to experience significant loss of charge collection efficiency indicating a possible upper limit in their usefulness under very high rates [16]. These results were obtained with diamond detectors significantly thicker (about 300–500 μm) than the ones presented here (4.5 μm). An irradiation measurement was performed for the detector shown in Fig. 6 at the OSU research reactor. This detector was irradiated at the core of the reactor at 150 kWth power for one hour resulting in a total fluence of 1-MeV neutron equivalent of 10^{15} n/cm^2.

After a cooldown period the detector could be handled to allow a measurement of its pulse height distribution at the thermal neutron beamline under identical conditions as those used to obtain the results of Fig. 6. The results are shown in Fig. 7 where the curves represent the results before irradiation and after irradiation. The count rates after threshold are very close in each curve but the pulse height distribution is shifted to lower values by an estimated amount of about 250 keV.

Fig. 8 compares the charge collection efficiency measured with the 5 MeV α-source (^{210}Po) before and after irradiation of the detector. The before irradiation result is without the BN layer and to take this into account the results shown are normalized by the observed 250 keV shift. At the operational voltage of 11 V both curves are in saturation suggesting no significant loss in efficiency. Fig. 9 shows the pulse height distribution at 20 V obtained with the ^{210}Po source before and after irradiation scaled by the corresponding shift at 20 V (see Fig. 8). It has been reported that BN, which is also a semiconductor and a thermal neutron detector, can be significantly affected at 1 MeV neutron equivalent fluences $\geq 10^{15}$ n/cm^2 exhibiting a certain degree of amorphization [17]. This could affect the mean path of the charged particles in the BN layer but it is not clear that is responsible for the observed shift to lower pulse height. Other possible contributors could be damage after irradiation to the metal-diamond contacts.

5. Summary

Diamond diode detectors with thin BN neutron converter layers have been tested at a thermal neutron flux of about 4.4×10^6 n/s/cm^2. The performance of the detectors was as expected with consistent results for different BN layer thicknesses and crystal orientation. Results were shown for a ⟨100⟩ orientation detector covered with a BN layer of about 0.5 μm thick. It is shown that under the thermal neutron flux the detector pulse height distribution identifies the reaction products

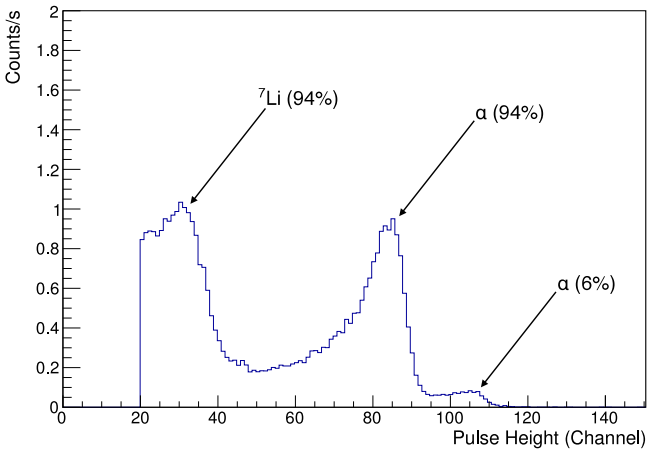

Fig. 6. Pulse height distribution. The horizontal axis is the charge collected per pulse and the vertical axis is the count rate for a detector in front of the 4.4×10^6 n/s/cm^2 thermal neutron beam. The arrows show the detection of the α and ^{7}Li particles from the 94% branching ratio and the α particle from the 6% branching ratio.

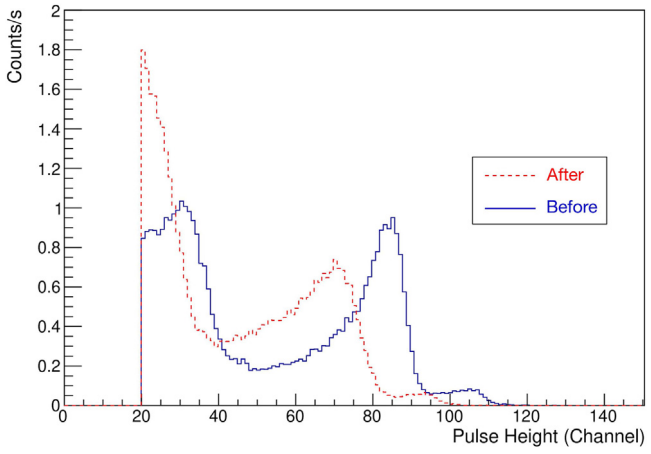

Fig. 7. Irradiation effect. The pulse height distribution for Fig. 6 detector in front of the thermal neutron beam before (solid line) and after (dashed line) irradiation by a 10^{15} n/cm^2 fluence.

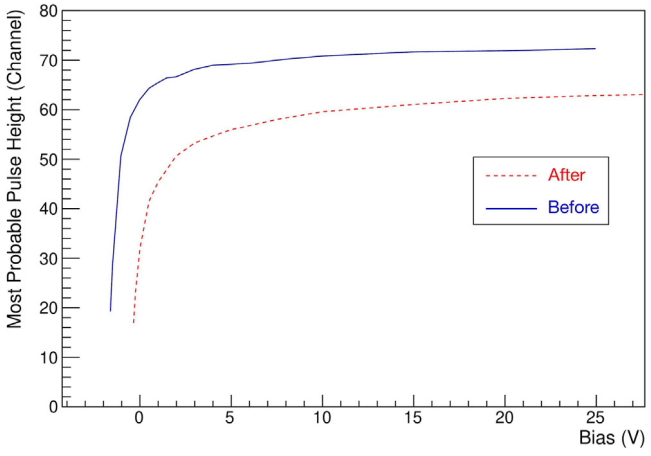

Fig. 8. Effect on charge collection. The relative charge collection efficiency before (solid line) and after (dashed line) the 10^{15} n/cm^2 irradiation.

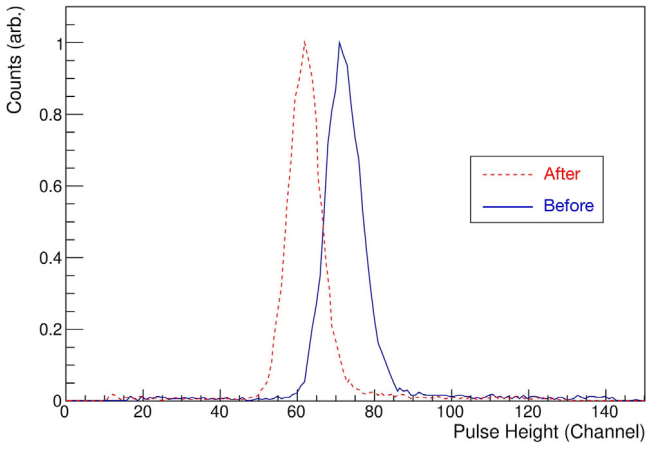

Fig. 9. Effect on pulse height. The pulse height distribution from a ^{210}Po source (5-MeV alpha particles) before (solid line) and after (dashed line) the 10^{15} n/cm^2 irradiation.

from the ^{10}B(n,α)^{7}Li neutron-capture reaction. The count rates were consistent with expected estimations. These measurements indicate that the tested detectors can operate in pulse counting mode up to fluxes of 10^9 n/s/cm^2 with the present data acquisition capabilities (160k counts per second). This count rate limit can be extended by about two orders of magnitude using faster available amplifiers and digitizers.

An irradiation test was performed for a 1 MeV neutron equivalent fluence of 10^{15} n/cm^2. Comparison of the results before and after irradiation showed a 250 keV shift to lower pulse heights at post irradiation with no significant change on the charge collection efficiency. The origin of the shift is a matter of further investigation.

Declaration of competing interest

The authors declare that they have no known competing financial interests or personal relationships that could have appeared to influence the work reported in this paper.

Acknowledgments

We acknowledge the support of Andrew Kauffman, Kevin Herminghuysen, and Dr. Susan White at The Ohio State University Nuclear Reactor Laboratory. This work was supported by ARPA-E, United States of America through the SWITCHES program.

References

[1] Douglas S. McGregor, R.T. Klann, H.K. Gersch, Y.H. Yang, Thin-film-coated bulk GaAs detectors for thermal and fast neutron measurements, Nucl. Instrum. Methods Phys. Res. A 466 (1) (2001) 126–141.
[2] S. Seshadri, Abdul R. Dulloo, Frank H. Ruddy, John G. Seidel, L.B. Rowland, Demonstration of an SiC neutron detector for high-radiation environments, IEEE Trans. Electron Devices 46 (3) (1999) 567–571.
[3] D.S. McGregor, M.D. Hammig, Y.-H. Yang, H.K. Gersch, R.T. Klann, Nucl. Instrum. Methods Phys. Res. A 500 (2003) 272–308.
[4] A. Maity, S.J. Grenadier, J. Li, J.Y. Lin, H.X. Jiang, J. Appl. Phys. 123 (2018) 044501.
[5] Y. Sato, H. Murakami, Japan. J. Appl. Phys. 54 (2015) 096401.
[6] J.H. Kaneko, et al., NIM A 505 (2003) 187.
[7] J. Holmes, M. Dutta, F. Koeck, M. Benipal, J. Brown, B. Fox, R. Hathwar, H. Johnson, M. Malakoutian, M. Saremi, A. Zaniewski, R. Alarcon, S. Chowdhury, S. Goodnick, R. Nemanich, Nucl. Instrum. Methods Phys. Res. A 903 (2018) 297.
[8] J. Holmes, M. Dutta, F. Koeck, M. Benipal, R. Hathwar, J. Brown, B. Fox, H. Johnson, A. Zaniewski, R. Alarcon, S. Chowdhury, S. Goodnick, R. Nemanich, Diam. Relat. Mater. 94 (2019) 162.
[9] G.F. Knoll, Radiation Detection and Measurement, John Wiley, Hoboken, N.J, 2010.
[10] W.J. Zhang, Y.M. Chong, I. Bello, S.T. Lee, J. Phys. D: Appl. Phys. 40 (2007) 6159–6174, 1.
[11] W.J. Zhang, et al., Angewandte Chemie International Edition 44 (2005) 4749–4753, 1.
[12] J. Shammas, T. Sun, F.A.M. Koeck, A. Rezikyan, R.J. Nemanich, Diam. Relat. Mater. 56 (2015) 13–22.
[13] A. Jablonski, J. Zemek, Surface and Interface Analysis 41 (2009) 193–204.
[14] D. Turkoglu, L. Cao, R. Lewandowski, Physics Procedia 43 (2013) 54–65.
[15] M. Wielunski, et al., Nucl. Instrum. Methods Phys. Res. A 517 (2004) 240–253.
[16] F. Kassel, M. Guthoff, A. Dabrowski, W. de Boer, Phys. Status Solidi A 214 (2017) 1700162.
[17] F. Cataldo, S. Iglesias-Groth, J. Radioanal. Nucl. Chem. 313 (1) (2017) 1–11.